Comparison of aerosol optical depth from satellite (MODIS), sun photometer and broadband pyrheliometer ground-based observations in Cuba.

Juan Carlos Antuña-Marrero[1], Victoria Cachorro Revilla[2], Frank García Parrado[1], Ángel de Frutos Baraja[2], Albeth Rodríguez Vega[1], David Mateos[2], René Estevan Arredondo[3,1], Carlos Toledano[2]

[1] Atmospheric Optics Group of Camagüey (GOAC), Meteorological Institute of Cuba, Camagüey, Cuba
[2] Atmospheric Optics Group (GOA), University of Valladolid (UVA), Valladolid, Spain
[3] Huancayo Observatory, Geophysical Institute of Peru, Huancayo, Peru

Resubmitted to *Atmospheric Measurement Techniques*

March 2018

Corresponding author:

Juan Carlos Antuña-Marrero

Atmospheric Optics Group of Camagüey

Meteorological Institute of Cuba

Camagüey, Cuba

Email: jcam45@gmail.com

Abstract

In the present study, we report the first comparison between the aerosol optical depth (AOD) and Angstrom exponent (AE) of the MODerate resolution Imaging Spectroradiometer (MODIS) instruments on the Terra (AOD_t) and Aqua (AOD_a) satellites and those measured using a sun photometer (AOD_{SP}) at Camagüey, Cuba, for the period 2008 to 2014. The comparison of Terra and Aqua data includes AOD derived with both Deep Blue (DB) and Dark Target (DT) algorithms from MODIS Collection 6. Combined Terra and Aqua (AOD_{ta}) data were also considered. Assuming an interval of ±30 minutes around the overpass time and the area of 25 km around the sun photometer site, two coincidence criteria were considered: individual pairs of observations, and both spatial and temporal mean values, which we call collocated daily means. The usual statistics (BIAS, MAE, RMSE) together with linear regression analysis are used for this comparison. Results show very similar values for both coincidence criteria: DT algorithm generally displays better statistics and higher homogeneity than the DB algorithm in the behaviour of AOD_t, AOD_a, AOD_{ta} as compared to AOD_{SP}. For collocated daily means: a) mean square errors (RMSE) of 0.060 and 0.062 were obtained for Terra and Aqua with the DT algorithm and 0.084 and 0.065 for the DB algorithm; b) MAE follows the same patterns; c) BIAS for both Terra and Aqua presents positive and negative values but its absolute values are lower for the DT algorithm; d) Combined AOD_{ta} data also give lower values of these three statistical indicators for the DT algorithm; e) both algorithms present good correlations for comparing AOD_t, AOD_a, AOD_{ta} vs. AOD_{SP}, with a slight overestimation of satellite data compared to AOD_{SP}, f) DT algorithm yields better figures with slopes of 0.96 (Terra), 0.96 (Aqua) and 0.96 (Terra+Aqua) compared to the DB algorithm (1.07, 0.90, 0.99) that displays greater variability. Multiannual monthly means of AOD_{ta} establish a first climatology more comparable to that given by the sun-photometer and their

statistical evaluation reveals better agreement with AOD_{SP} for the DT algorithm. Results of the AE comparison showed similar results to those reported in the literature concerning the two algorithms' capacity for retrieval. A comparison between broadband optical depths (BAOD), derived from broadband pyrheliometer observations at the Camagüey site and three other meteorological stations in Cuba, and AOD observations from MODIS on board Terra and Aqua show a poor correlation with slopes below 0.4 for both algorithms. Aqua (Terra) showed RMSE values of 0.073(0.080) and 0.088(0.087) for the DB and DT algorithms. As expected, RMSE values are higher than those from the MODIS/sun photometer comparison, but within the same order of magnitude. Results from the BAOD, derived from solar radiation measurements, demonstrate its reliability to describe climatological AOD series estimates.

KEY WORDS: atmosphere, remote sensing, aerosols, Aerosol Optical Depth (AOD), Broadband Aerosol optical depth (BAOD), AERONET, MODIS

1. Introduction

Atmospheric aerosols play an important role in weather and climate (IPPC 2013). Depending on the physical/chemical and optical properties of atmospheric aerosols together with their origin and spatial and temporal distribution, they can affect the Earth's radiative budget, as well as dynamic, biogeochemical and chemical processes (Knippertz and Stuut, 2014; Seinfeld and Pandis, 2016). All of these processes play a key role at a global and regional scale due to the high spatio-temporal variability of aerosol properties. Aerosols can also affect the biosphere and, in particular, humans in several ways: for example, the Saharan dust transported to America across the Atlantic supplies nutrients to the Amazon forest (Swap et al., 1992; Yu et al., 2015). Moreover, in the Caribbean, in

addition to aerosols of local origin, dust makes the amount of aerosol exceed air quality standards associated to human health (Prospero and Lamb, 2003; Prospero et al., 2014). The great variability of Saharan dust transported to the Caribbean basin has been documented using long-term observations in Barbados (Prospero and Lamb, 2003; Prospero and Mayol-Bracero, 2013) and more recently in Miami, Guadeloupe and Cayenne (Prospero et al., 2014). The Caribbean region is thus of great importance for aerosol studies due to its low aerosol background, which helps aerosol transport studies (Kaufman et al., 2005; Denjean et al., 2016; Velasco et al., 2018). One difficulty, however, is that it is an area where land and water make up a mixed pixel when remote satellite aerosol studies are carried out.

In order to improve calculations of aerosol climatology for Cuban land areas, which remains ongoing, we compared aerosol ground-based observations and available satellite data, as a first step towards assessing this climatology. This involves a comparison between all the available Camagüey sun photometer aerosol optical depth (AOD) data and the BAOD provided by solar radiation measurements with the series of AOD (550 nm) from the MODerate resolution Imaging Spectroradiometer (MODIS) instruments on board the Terra (2001 to 2015) and Aqua (2002 to 2015) satellites. Selected observations were those spatially and temporally collocated between satellite instruments and ground-based sites. In addition to the aerosol load given by the AOD, we also evaluated the Ångström exponent (AE) as a parameter providing information about particle size for MODIS and sun photometer data.

One of the challenges we faced was the low amount of potential coincident AOD and AE from MODIS and the Sun photometer. The same is true for AOD from MODIS and broadband pyrheliometer derived BAOD, in both cases due to existing gaps in the ground-based time series and also because this area is strongly affected by clouds (mainly partially cloud cover). In order to

maximize the number of satellite and surface measurement pairs, we used primary AOD and AE L2 products without any averaging as well as combined AOD and AE from Terra and Aqua MODIS sensors as a whole dataset. We also used Deep Blue (DB) and Dark Target (DT) algorithms to evaluate the reliability of satellite AOD and AE retrievals to select the most appropriate data set to derive the climatology of both AOD/AE aerosol parameters in Cuba.

The earliest attempt to measure aerosol optical properties at ground level in Cuba recorded in a scientific publication dates back to 1988 (Martinez, 1988) where the Linke turbidity factor and the Ångström ß turbidity coefficient were derived from solar direct normal irradiance (DNI) measurements. Twenty years later, a cooperation agreement between scientific institutions in Spain and Cuba enabled a Cimel CE-318 sun photometer to be installed at Camagüey (Cuba) and for it to be included in the Aerosol Robotic Network (AERONET, Holben et al., 1998). Several aerosol studies have been conducted using the Aerosol Optical Depth (AOD) and AE from Camagüey's sun photometer observations (see, Antuña-Marrero et al., 2016; http://www.goac.cu/uva/).

Broadband pyrheliometric DNI observations allow the Broadband Aerosol Optical Depth (BAOD) to be determined, which complements sun photometer aerosol observations at Camagüey, and provides aerosol information at three other locations in Cuba. The main purpose of determining BAOD is to offer information concerning aerosol variability over the island, also making it possible to extend aerosol records back in time. The first BAOD calculations used for DNI measurement were conducted at Camagüey under clear sky conditions for the period 1985-2007 using Gueymard's (1998) improved parameterizations (Fonte and Antuña, 2011). García et al. (2015) used this kind of DNI observation for a longer period (1981-2013) and compared this BAOD to sun-photometer AOD data. They used observations under the clear line of sight between

125 the broadband pyrheliometer and a region of 5° around the Sun, as well as improved climatological
126 values of the integrated water vapor.

127 This comparative analysis does not aim to be a validation study of the MODIS sensor since
128 many works during the long history of the MODIS sensor on the Terra and Aqua platforms have
129 sought to improve its features (these include: Kaufman et al., 1997a, b; Tanré et al., 1997; Remer
130 et al., 2002, 2005, 2006; Hsu, et al., 2004,2006, 2013; Levy et al., 2007; 2009; 2010, 2013, 2015;
131 Sayer et al., 2013, 2014; https://darktarget.gsfc.nasa.gov/atbd/overview). However, compared to
132 other areas of the world, no studies have been reported in the Caribbean region and in Cuba in
133 particular (Papadimas et al., 2009; Mishchenko, et al., 2010; Kahn et al., 2011; Bennouna et al.,
134 2011, 2013; Witte et al., 2011; Gkikas et al., 2013; 2015; Levy et al., 2015).

135 As mentioned, our aim is to establish reliable aerosol climatology in Cuba based on satellite
136 and ground-based instruments. By making a detailed comparison of similarities and differences
137 between available data sets, the present work seeks to make a contribution to said aim.

138 The article is structured as follows. Section 2 begins with the description of the datasets,
139 followed by the explanation of the coincidence criteria between the AOD and AE MODIS L2
140 products and the same two variables from the sun photometer and broadband pyrheliometer
141 BAOD. This section ends with the explanation of the statistical indices used. Section 3 is composed
142 of various sections designed to explain and discuss the large volume of results to emerge from the
143 comparison given by taking two different retrieval AOD aerosol algorithms, for both the Terra and
144 Aqua platforms, with the sun photometer and BAOD. Section 4 contains a summary of the
145 conclusions.

146

147 **2. Materials and Methods**

148 **2.1** ***MODIS satellite instruments***

149 The twin MODIS instruments on board the Terra and Aqua satellites have accumulated
150 over 15 years of observations of several atmospheric parameters, including AOD at several
151 wavelengths and the AE parameter, the two most common parameters for describing atmospheric
152 aerosol optical properties. Based on the assumptions about the properties of the Earth's surface
153 and the aerosol type expected over these surfaces, the MODIS Atmosphere team developed three
154 algorithms for processing MODIS observations (Levy et al., 2013). Regions which appear visually
155 "dark" from space, referred to as Dark Target (DT), include the algorithm assumptions for
156 vegetated land surfaces (Kaufman et al., 1997a, b) and for remote ocean regions (Tanré et al.,
157 1997). The third algorithm, called the Deep Blue (DB) algorithm, includes assumptions for
158 surfaces which are visually "bright" from space and uses near-UV wavelengths (DB band near 410
159 nm). Under these conditions, the DB band provides a better signal than the visible wavelengths,
160 improving the information content for aerosol retrievals (Hsu et al., 2004; 2006) due to lower
161 surface albedo at this short wavelength. Levy et al. (2013) provide a detailed explanation of basic
162 MODIS retrieval concepts and improvements to the DT algorithm in Collection 6 for aerosol
163 products. In addition, Hsu et al. (2013) give a detailed explanation of the DB algorithm
164 improvements in Collection 6.

165 Following Levy et al. (2013), we summarize the MODIS calculus chain. MODIS Level 0
166 (L0) is the basic data file containing raw observations from the sensors. Observations grouped in
167 five-minute swath scans (called granules) are Level 1A (L1A), which after calibration becomes
168 Level 1B (L1B). L1B data feed the MODIS geophysical retrieval algorithms, generating the
169 primary geophysical observations, which include AOD and AE, designated Level 2 (L2). This is
170 followed by Level 3 (L3), consisting of daily and monthly statistics of geophysical products, in 1º

171 x 1º latitude\longitude grid boxes. L2 aerosol products are stored in the MOD04 (Terra) and
172 MYD04 (Aqua) files.

173 We selected AOD at 550 nm from MODIS (both on Terra and Aqua satellites) Collection
174 6, L2 data level derived using the two algorithms; DB for land with the highest data quality
175 (Quality flag = 2, 3) and DT for land, corrected (Quality flag = 3). In addition, we selected the AE
176 retrieved over land from the DB algorithm using the corresponding pairs of AOD values (412/470
177 nm or 470/650 nm) with the highest quality (Quality flag = 2, 3), since the DT algorithm only
178 retrieves the AE over the ocean (Table B1 in Levy et al., 2013). Table 1 lists the aerosol products
179 used in the present study.

180 At a global scale, it has been established that using the DT algorithm over land, MODIS-
181 retrieved aerosol size parameters evidence poor quantitative capacity, particularly AE (e.g., Levy
182 et al., 2010; Mielonen et al., 2011). However, for the DB algorithm, AE capacity increases for
183 moderate or high aerosol loadings, AOD > 0.3 (Sayer et al., 2013). We therefore decided to
184 conduct the comparison between the AE from the MODIS DB algorithm and the AE from the
185 Camagüey sun photometer to estimate its uncertainty. The enhanced DB algorithm methodology
186 for deriving AE in Collection 6 is the same as in Collection 5. It uses the Ångström power law and
187 AOD values at 412, 470 and 650 nm. Under non-vegetated surfaces, AE is derived using the AOD
188 from pair 412/470 nm. For vegetated surfaces, AE is derived from the 470/650 nm pair. In the case
189 of a surface with mixed vegetated and non-vegetated areas, AE is derived using the AOD at the
190 three wavelengths mentioned (Hsu et al., 2013).

191

192

193 **2.2 *Camagüey AERONET sun-photometer***

194 The Camagüey sun photometer, installed thanks to an agreement between the University
195 of Valladolid (UVA), Spain, and the Meteorological Institute of Cuba (INSMET) for joint aerosol
196 research, contributes to the NASA Aerosol Robotic Network (AERONET) (Antuña et al., 2012).
197 Annual replacement of the instrument for one calibrated, sent from Valladolid to Camagüey,
198 encountered numerous transportation and customs delays, causing gaps in the observation series.
199 However, the collected series of observations does represent a valuable dataset of aerosol columnar
200 optical properties in the Caribbean, enabling GOAC-INSMET and GOA-UVA to conduct
201 preliminary aerosol research (Antuña-Marrero et al, 2016).

202 The AERONET Cimel sun photometers have been conducting aerosol observations at nine
203 spectral narrow band filters for over two decades, producing spectral AOD and column effective
204 particle properties (Holben et al., 1998). In general, Cimel sun photometer nominal wavelengths
205 are 340, 380, 440, 500, 675, 870, 935, 1020 and 1640 nm. In some cases, the 1640 nm is replaced
206 by a 1240 nm. Its processing algorithm, based on the Beer-Lambert-Bouguer law, allows spectral
207 OD values at an uncertainty level of approximately 0.01 to 0.02 to be determined (Holben et al.,
208 1998; Eck et al., 1999). Because of this low level of uncertainty, AERONET AOD observations
209 commonly serve as reference values ("ground truth") to validate AOD measured by other remote
210 sensing sensors (Zhao et al., 2002). AERONET AE are derived for five different wavelength
211 intervals; 340-440 nm, 380-500 nm, 440-675 nm, 440-870 nm and 500-870 nm. In the present
212 study, the selected AE is the one in the 440-675 nm range (AE_{SP}).

213 We used Camagüey sun photometer Level 2.0 data as processed by AERONET, i.e., cloud
214 screened and quality-assured (Smirnov et al., 2000), covering the period from 7 October 2008 to
215 1 August 2014. This consisted of 29,940 single AOD (340 to 1640nm) and AE_{SP} observations.

Applying the Ångström power law, we converted single sun photometer AOD observations at 500 nm wavelength to AOD at 550nm, (AOD_{SP}) using the AE_{SP} from the same measurement:

$$AOD_{SP} = AOD_{500}\left(\frac{\lambda_{550}}{\lambda_{500}}\right)^{-AE_{SP}} \quad (1)$$

2.3 *Solar direct irradiance measurements and derived Broadband Aerosol Optical Depth(BAOD)*

Four actinometrical stations belonging to the "Diagnostic Service for Solar Radiation in Cuba" provided the DNI observations used to derive the BAOD (Antuña et al., 2008; 2011). Table 2 lists the WMO code of the four stations, the geographical location and the number of observations available for the periods at each station. Figure 1 shows the geographical location of the four stations. The stations are equipped with Yanishevsky manual broadband solar radiation instruments supplied between the 1970s and 1980s by the Hydrometeorological Service of the Soviet Union. The Yanishevski broadband pyrheliometer is the M-3 model, a thermo-battery system with a 5º field of view connected to an analogic galvanometer, GSA-1MA or GSA-1MB model (GGO, 1957).

Calibrations of all the actinometrical instruments are conducted periodically by comparison with a master broadband pyrheliometer and a master pyranometer. Trained observers perform hourly manual observations from sunset to sunrise, following the standard methodologies and quality control procedures established for this set of instruments (GGO, 1957). Once manual measurement is conducted and recorded in a notebook designed for the purpose, all the measurement information is digitized using Actino version 2.0 software (Estevan, 2010; Antuña et al., 2008) of the "Diagnostic Service of the Broadband Aerosol & Clouds Optical Depth for

Cuba" (http://www.goac.cu/eoc/), a public service provided by GOAC. The software includes a robust quality control of input data, its processing and output quality control (Antuña et al., 2011). Because of the ageing of the Soviet era instruments, the magnitude of the error associated to the broadband pyrheliometers currently operating in Cuba is estimated to be around 10 %.

Based on the model parameterization of solar broadband irradiances, the integrated aerosol optical depth δ_a, BAOD, can be obtained using equation (2), where direct normal solar irradiance (DNI) is measured and the remaining variables are determined independently (Gueymard, 1998).

$$\delta_a = \left(\frac{1}{m_a}\right)\left[ln\left(\frac{E_{0n}}{DNI}\right) - m_R\delta_c - m_w\delta_w - m_{nt}\delta_{nt}\right] \qquad (2)$$

The individual atmospheric processes considered are: Rayleigh scattering, absorption by ozone (O_3), stratospheric and tropospheric nitrogen dioxide (NO_2), uniformly mixed gases, water vapor, and extinction (mostly scattering) by aerosols. The variables in equation (2) are: optical air mass of aerosols (m_a), Rayleigh scattering, uniformed mixed gases, O_3 absorption and stratospheric NO_2 (m_R), water vapor (m_w) and tropospheric NO_2 (m_{nt}) and similarly the corresponding broadband optical depths δ. The method makes a series of assumptions, i.e., Bouguer's law; in the strict sense that it is only valid for monochromatic radiation and is applied to define broadband transmittance. For a detailed description of the derivation of equation (2) and the parameterization of the variables, see Gueymard, (1998), and Fonte and Antuña (2012) and García et al. (2015) for the method's application to our data.

In order to avoid cloud contamination in BAOD retrieval, we used only DNI observations with the cloud-free condition in the line of sight to the sun, in other words with a clear line of sight between the broadband pyrheliometer and a region of 5° around the sun (GOAC, 2010). Furthermore, to avoid errors associated with high elevation zenith angles, causing larger air

masses, DNI observations performed at 6:00 and 18:00 Local Time (LT) were not used in the present study.

The main errors of the method for determining BAOD are associated to instrumental errors and the error when estimating the precipitable water (PW) component (Gueymard, 2013). In the first case, in order to ensure the quality of the solar radiation dataset from the four actinometrical stations used in this study, including DNI, they are regularly subject to a two-step quality control (Estevan et al., 2012). The first step applies the standard procedures designed for Yanishevski type actinometrical instruments from the former Soviet Hydro-Meteorological Service (Kirilov et al., 1957). Data that pass this quality procedure are then evaluated following the standards set by the Baseline Solar Radiation Network - BSRN (Ohmura 1998, Long and Shi, 2006; 2008; Estevan et al., 2012).

The size of the field of view of the broadband pyrheliometers is another potential source of error since, in certain cases, circumsolar radiation causes more radiation to be measured than expected. In such cases, the effect is an underestimation of BAOD. Nevertheless, this effect is low in general, except in specific conditions such as large air masses, in the presence of high aerosol loads or of large-particle aerosols (Gueymard, 1998).

Monthly mean PW values at the four actinometrical stations were used as input to derive monthly mean δ_w values (Gueymard, 1998). For Camagüey, we calculated the monthly mean PW values from the sun photometer PW observations from 2008 to 2014 (García et al., 2015). For each of the three other stations, we calculated the monthly mean PW values using the vertical integrated water vapor (kg m^{-2}) from spatially coincident ERA-Interim reanalysis between 1979 and 2013 (Barja et al., 2015). Taking into account all the above-mentioned errors, the total uncertainty of the method used to determine BAOD is in the order of 10^{-2} (Gueymard, 1998).

2.4 *Coincidence criteria for MODIS and Sun photometer observations*

Obtaining sufficient AOD satellite observations over land for climatological studies in insular areas poses a challenge when compared to the amount of data usually available over continental regions such as the US, Europe or China. The reason tends to be the small size of the islands. In the case of Cuba, its particular narrow latitudinal and elongated longitudinal extension combined with its irregular coasts renders the MODIS L3 product unsuitable for climatological studies. As can be seen in Figure 1, most of the 1º by 1º grid cells consist of both land and sea areas, resulting from the merging AOD measured over the two surfaces. The red grid cell in Figure 1 is an example of the limitations of MODIS L3 products to represent land areas in the case of Cuba. In response to this, we plan to use the MODIS L2 product to produce aerosol climatology for Cuba rather than L3, which is commonly used for this type of studies. In this regard, it is vital to validate the single observations from MODIS L2 with the single sun photometer observations. We designed and applied a method to maximize the available pairs of MODIS L2 and sun photometer AOD and AE observations coincident in space and time, avoiding duplicating the use of any of them. Additionally, in an effort to increase the amount of data, we tested the differences between Terra and Aqua L2 MODIS AOD and AE observations in order to determine the possible combination of both Terra and Aqua in a single dataset.

Hereinafter, AOD_t, AOD_a, AOD_{ta} and AOD_{SP} will denote spatio-temporal AOD from collocated MODIS (Terra, Aqua and Terra + Aqua) and AERONET sun photometer data, respectively. Unless otherwise indicated, "AOD" refers to AOD at 550 nm wavelength. Similarly, AE from Terra, Aqua and Terra + Aqua derived using only the DB algorithm will be denoted as AE_t, AE_a and AE_{ta}.

306 Given the challenges arising from the small amount of potential coincident spatial and
307 temporal AOD_t and AOD_a with AOD_{SP} and BAOD, as explained above, we used MODIS L2 data
308 to maximize the amount of available MODIS observations for comparison. Hereinafter, we call
309 these observations "single observation values"; using the same denomination for the instantaneous
310 sun photometer observations on each day and for hourly broadband pyrheliometer observations.
311 Another way to increase the amount of data was to combine AOD_t and AOD_a (AOD_{ta}) for
312 comparison with AOD_{SP} and BAOD. In these cases, different observations of AOD_{SP} and BAOD
313 match AOD_t and AOD_a because the time difference established for coincidence (± 30 min) is lower
314 than the difference between the Terra and Aqua daily overpass times.
315 Spatial coincidence criteria were guaranteed by selecting all the AOD_t and AOD_a measured
316 inside the 25 km radius around the sun photometer site for the whole data period from each satellite
317 sensor. Table 3 shows the amount of spatial coincident information for non-negative AOD_t and
318 AOD_a values. It shows the amount of data available for the whole period 2001 to 2015, when
319 broadband pyrheliometer observations at Camagüey are available, and 2008 to 2014, the period of
320 available sun photometer observations. There are at least twice as many available observations
321 from Terra as from Aqua for the two periods. The greater number of available data from Terra
322 compared to Aqua is associated to the different overpass times of the two satellites over Cuba.
323 Figure 2 shows that Terra overpasses occur in the mid to late morning before convective activity
324 begins, while the Aqua overpasses take place in the early afternoon when convection has already
325 begun, causing a higher number of observations to be discarded in AOD retrievals due to cloud
326 presence.

327 **2.4.1 Collocated "*Single observation" values and "daily mean" values***

All Aqua and Terra overpass times in a radius of 25 km around Camagüey for the periods 2001 to 2015 (Terra) and 2002 to 2015 (Aqua) are shown in Figure 2. Overpass times, defined by the maximum and minimum values of all the 25 km spatially coincident MODIS observations, are 10:12 – 11:49 (LT) for Terra and 12:47 – 14:20 (LT) for Aqua. In addition, Figure 2 shows the diurnal frequency of sun photometer observations from 2008 to 2014, and the diurnal frequency of the BAOD observations for Camagüey for the period 1981 to 2015. Note that the BAOD histogram shows only hourly frequency values, since that is the time interval between the manual pyrheliometric observations.

For each day, we compared the corresponding time of each single sun photometer measurement with the time of each single AOD_t and AOD_a observation located in a radius of 25 km around the sun photometer site (an area of almost 2,000 km^2) and in the time window of ± 30 minutes between both types of observations. The former selection process includes, for each satellite, the AOD_t and AOD_a values derived both with the DB and DT processing algorithms separately, producing four independent bulk datasets, two for Aqua and two for Terra. We then identified four different cases of matching data per day in the bulk coincident datasets. The first consisted of days with only one AOD_{SP} value and one AOD_t (AOD_a) coincident value, and the second, only one AOD_{SP} value coincident with multiple AOD_t (AOD_a) values each day. In the third case, only one AOD_t (AOD_a) value coincided with multiple AOD_{SP} values. Finally, the fourth case consisted of multiple AOD_{SP} values coincident with multiple AOD_t (AOD_a) values.

Coincident cases were then selected for comparison, case by case. In the first instance, we selected all cases. In the second case, because of the MODIS instruments spatiotemporal sampling geometry, time differences between MODIS and sun photometer observations are in the order of one minute. As a result, only the criterion of the minimum distance between the positions of the

351 AOD_t (AOD_a) and the sun photometer was applied to determine the pair of coincident values,
352 therefore not allowing any repeated AOD_{SP} and AOD_t (AOD_a) values to be selected. Since it
353 consists of only one AOD_t (AOD_a) measurement and multiple AOD_{SP} observations, in the third
354 case the distance is the same; hence the selection criteria was the minimum of the time differences
355 between AOD_{SP} and AOD_t (AOD_a) observations. The fourth case, the most complicated, allowed
356 both criteria to be applied; the minimum in distance and time. No differences in the amount of
357 coincident data were found when testing whether the order in which the two criteria were applied
358 had any impact.

359 Another approach, the most commonly used for comparison (Bennouna et al., 2011; Sayer
360 et al., 2014), involves the average of all the AOD_{SP} values in the interval of ± 30 minutes compared
361 to MODIS instrument overpass time (note that AOD_t and AOD_a averages are really the daily values
362 of MODIS) located in a radius of 25 km around the sun photometer. At least two single AOD_{SP}
363 and two single AOD_t (AOD_a) observations were required to calculate the spatio-temporal average.
364 We applied a similar approach to calculate collocated daily means AE_{SP}, AE_t and AE_a. The
365 procedures described above generated a series of collocated daily means of AOD_{SP} versus AOD_t
366 (AOD_a) and AE_{SP} vs. AE_t (AE_a). Hence, by combining the former generated series of AOD (AE)
367 for Terra and Aqua we produced the coincident (Terra + Aqua) dataset. The term *collocated daily*
368 *mean AOD* will be used hereinafter although it should be stressed that this approach reduces the
369 number of observations generated by virtually a third.

370 After explaining the coincidence criteria adopted here, it is well known that this type of
371 comparison shows major differences depending on the spatial and or temporal resolution taken for
372 the MODIS sensor in relation to the ground-based instruments used (Santese et al., 2007; Levy et
373 al., 2009; Bennouna et al., 2011, 2013). The justification for using a "single observations" dataset

and a “collocated daily means” dataset separately to analyze this comparison is based on: a) the characteristics of the surface area under study, with nearby areas of water and land; b) the difference concerning how cloud cover affects data during the overpass time of the Terra and Aqua platforms; and c) the possibility of including the largest amount of data; d) the fact that only single observations can be compared in the case of BAOD pyrheliometer measurements.

2.5 *Statistics*

The statistics used in the present study are those commonly used (e.g., Sayer et al., 2014). These are the root mean square error (RMSE), mean absolute error (MAE), median bias (BIAS), the Pearson linear correlation coefficient (R), the number of coincident MODIS and sun photometer cases (Cases) and the fraction (f) of the MODIS/AERONET AOD retrievals in agreement within the expected uncertainty. Expected uncertainty, defined as a one standard deviation confidence interval entails the sum of the absolute and relative AOD errors. Usually referred to as “expected error, EE”, it was applied in accordance with equation 3 (Sayer et al., 2014)

$$EE_{DT} = \pm(0.05 + 0.15\,AOD) \quad (3)$$

The aim is to compare the performance of the DB and DT algorithms directly (Sayer et al., 2014). All of these statistical indicators were evaluated for the whole set of collocated AOD_t, AOD_a, AOD_{ta} with AOD_{SP}, and BAOD; AE_t, AE_a, AE_{ta} with AE_{SP}; as well as time frequencies (Figure 2) and histograms of these quantities. We also evaluated these statistics on a monthly scale for the AOD values.

3. Results and Discussion.

This section is divided into four subsections. In the first subsection, we analyze in detail the main results from comparing the AOD satellite MODIS sensors and the sun photometer data given by the statistical indicators and linear correlations, as a result of taking two different criteria, two different retrieval AOD aerosol algorithms both for the Terra and Aqua platforms. Section 3.2 analyzes the same type of results but under the perspective of monthly values since they represent the climatology of AOD and the associated uncertainties. Section 3.3 shows AE behavior and Section 3.4 analyzes the comparison of satellite MODIS data in relation to broadband aerosol optical depth from solar radiation.

3.1 ***Comparison of AOD retrievals from sun photometer and MODIS satellite instruments.***

As explained, we selected MODIS AOD_t (AOD_a) and sun photometer AOD_{SP} data based on two different criteria for their comparison. Results are shown in Tables 4 and 5, corresponding to collocated daily means and single observations , respectively. The values of all the statistics of these two tables are extraordinarily similar, with analogous behavior for the different algorithm and platforms. In truth, no substantial differences are found. It must be noted that Table 4 for collocated daily means contains a third less data than Table 5 based on single observations. In contrast, however, the latter data have a higher associated error than daily mean data. This result cannot be foreseen a priori but clearly demonstrates that either criterion may be taken, since the result is basically the same.

Taking Table 5 together with Figure 3 of collocated daily mean values, we then analyze the different behavior of the two algorithms for the Terra and Aqua platforms, when AOD_t (AOD_a) from satellite are compared with the sun photometer, AOD_{SP}. Figure 3 shows the density plots of the collocated daily mean AOD values from the sun photometer versus those of MODIS instruments for Terra, Aqua and combined, for DB (top plots) and DT (bottom plots) algorithms.

The least squares linear fit lines and equations are also shown in the figure while the correlation coefficients (R values) are in Table 5. In general, the plots show that low loading aerosols predominate and that scatter increases for higher aerosol loadings, with a slight overestimation of AOD_t (AOD_a) satellite data compared to AOD_{SP}. In all cases, the slopes are between 1 and 0.9 and the intercepts are in the order of 10^{-2} (with lower values for the DT algorithm), showing very good values of these parameters for Terra and Aqua for both the DT and DB algorithms.

Figure 3 shows that the DT algorithm displays generally better behavior than the DB algorithm. The DT algorithm evidences more unified behavior as can be seen for the slope values (0.96 for both Aqua and Terra) while DB changes, giving a value above 1 (1.069) for Terra and below 1 for Aqua (0.901). However, these differences are not very relevant since both algorithms give almost identical R values, and the difference appears for the platforms, with higher values for Aqua than for Terra (~0.78 and ~0.73, respectively). A compensation effect can be observed when data are combined, since in this case the slope of the DB algorithm is closer to 1 than the DT algorithm, although the intercept is higher (closer to 0 for DT algorithm). For combined data, the two algorithms show a more similar behavior than for separate Aqua or Terra results. Analyzing Table 5, the magnitudes of the RMSE, MAE, BIAS and f statistics are lower for the DT than for the DB algorithm (see the higher values of DB for Terra, column 1, and the more similar values in the other columns). As mentioned, the values of these four parameters show that the DT algorithm presents a more unified behavior for both platforms than the DB, which has similar values for Aqua but which change significantly for Terra.

Although the statistical numbers in the comparison depend on the area under study, comparisons between areas are always possible. A recent validation of MODIS Collection 6 AOD_a (Aqua), derived using the DB algorithm, with AOD_{SP} from six AERONET stations in

Central/South America (CSA) and seven in Eastern North America (ENA) was reported by Sayer et al. (2013). The number of pairs of collocated MODIS and AERONET daily averaged observations for CSA (ENA) was 3,032 (4155). Sun photometer data were averaged within the 30 minute MODIS overpass time and MODIS data were averaged in the 25 km radius around the sun photometer site, which makes the comparison appropriate. We selected the BIAS and R statistics in Table 1, which were defined as in the present study (Sayer et al., 2013).

We compare those statistics with the ones given in Tables 4 and 5, calculated for Camagüey. The BIAS for the CSA (ENA) stations is -0.016 (0.0094), although those of Camagüey for both single observations and collocated daily means are (-0.027 and -0.033), thus showing higher values for Camagüey and similar signs for CSA and the opposite for ENA. R values for Camagüey for single observations and collocated daily means are 0.82 and 0.79, respectively, lower by around 10 % (5 %) than the R values of 0.96 (0.86) for the CSA (ENA). However, it should be noted that the number of cases used for the statistics at Camagüey was 419 for single observation and 169 for collocated daily means, representing 6 % and 14 % of the 3,032 cases used in the cited study. In addition, none of the stations in the CSA (ENA) regions were located in the Caribbean, but south and north (Sayer, 2018). Despite the significant difference in the amount of cases used in both studies and the location of the six stations, results show reasonable agreement.

3.2 Monthly means values and statistics

Given the close similarity in the results from single observations and collocated daily means data, it seems reasonable to evaluate monthly mean values based on only one of them, i.e., for the collocated daily means data. Figure 4 shows the monthly means (based on the mean of each month for every year of the measured period) and the statistics resulting from the comparison between AOD_{SP} and AOD_{ta} for both the DB and DT algorithms. Tables S1 and S2 (see

supplementary material) also illustrate this comparison although they add separate information for Terra and Aqua (see supplementary material). In Figure 4a, the multiannual monthly means from the combined AOD_{ta} and AOD_{SP} for both the MODIS DB and DT algorithm are shown, providing an initial overview of aerosol AOD climatology in Camaguey. It can also be seen that the DT algorithm gives the best match with monthly mean AOD_{SP}.

The monthly RMSE and MAE plots in Figures 4b and 4c generally show increases, with the increase in the AOD_{ta} for the DT algorithm and also for the DB algorithm, the exception being the minimum in April for the DT algorithm (this means greater differences between satellite and sunphotometer in summer than in winter). These results are consistent with the fact that AOD uncertainty depends on the AOD itself (see eq. 3) and greater AOD variability in summer. The AOD_{ta} peaks for the DT algorithm in March in both RMSE and MAE are also present in the results for AOD_t and AOD_a, separately, and the amount of cases available for the statistics is among the highest of all the months seen in Tables S1 and S2 (see supplementary material). In Table S2, for the DT algorithm, we can see that the number of cases of AOD_{ta} from March to April drops by 55 %. However, something similar happens for the DB algorithm in Table S1, with the number of AOD_{ta} cases falling from March to April by 61 %. Sampling cannot therefore be seen as the cause of the RMSE and MAE peaks for the DT algorithm. We plan to revisit this feature in future studies. In summer, RMSE and MAE show their maximum values associated to the maximum values of the AOD resulting from Saharan dust reaching Cuba from across the Atlantic. The BIAS is negative in summer for both Terra and Aqua AOD, showing that AOD_t and AOD_a observations have higher magnitudes than AOD_{SP}.

Tabulated results of the comparison between AOD_t, AOD_a and AOD_{ta} with AOD_{SP} on a monthly scale also show better results for the DB (see Table S1) than for the DT (Table S2)

algorithm. Here, we only discuss the results of the joint AOD_{ta} dataset using both the DT and DB algorithms. In Figures 4d, the BIAS for the DT algorithm is positive from December to May, a period of the year with predominant lower AOD_{ta} and AOD_{SP} values. During this period, AOD_{ta} underestimates AOD_{SP}. BIAS then becomes negative from June to November, which is when Saharan dust reaches the Caribbean basins. At the same time, the BIAS of the AOD_{ta} derived with the DB algorithm is negative for the whole year, with higher absolute values than those from the DT algorithm.

The correlation coefficient, R, in Figure 4e is the statistic which shows almost the same agreement for the DB and DT algorithm. However, the DT shows a higher number of R-values bearing higher magnitudes. R magnitudes remain over 0.5 almost the whole year round except in December and January when lower AOD values occur.

Figure 4f shows the fraction of the AOD_{ta} (f), in agreement with AOD_{SP} within the expected uncertainty, showing its higher values over 80 % from November to January, in general for both algorithms. This is the period of the year with the lowest monthly mean values of both AOD_{ta} and AOD_{SP}. During the rest of the year, including the period of the Saharan dust arrivals, it shows its lowest values between 60 % and 75 % for the DT algorithm while values for DB below 50 % occur in four of the months between June and October. The discontinuous blue line at f = 68 % denotes a one standard deviation confidence interval, selected to describe EE. The f values above that value mean the algorithm works better than expected. All the statistics demonstrate that the DT algorithm performs better than the DB for the region of study. However, the lowest R values for those months with the highest f values would seem to be contradictory. At present, we have no explanation for this.

3.3 Comparison of Ångström Exponent by sun photometer and MODIS satellite instruments:

Figure 5 shows the frequency distribution of the coincident AE_{SP} with both AE_t and AE_a using the DB algorithm, as explained. As can be seen in the literature, the Ångström Exponent varies between 0 and 2. Our Ångström Exponent data obtained from the AERONET sun photometer measurements are within this range with a wide and smooth frequency distribution of values and with a not well-defined maximum in the range 1.2 and 1.6. Neither AE_t nor AE_a present any real distribution shape because there are practically no values below 1, with most being around AE = 1.5, followed by a second maximum at AE= 1.8. The first, 1.5, is a regional default value for AE_t and AE_a (Hsu et al., 2013; Sayer et al., 2013) assumed by the DB algorithm in the case of low AOD values (AOD_t or $AOD_a < 0.2$). The second is associated with the fact that the AE_t and AE_a values allowed by the aerosol optical models in Collection 6 are constrained between 0 and 1.8 to avoid unrealistic values (Sayer et al., 2013).

Table 6 shows the results of the comparison of coincident AE_t, AE_a and AE_{ta} with E_{SP}. For both single observations and collocated daily mean data the statistics were calculated for the two options: the first including all values and the second excluding cases with AE=1.5 and 1.8. The statistics in Table 6 for all values present similar values considering those derived by single observation or for collocated daily mean values as expected once we know the results for AOD, although similar values also appear for Terra and Aqua (no clear distinction appears between Terra and Aqua). These statistics present very high values if compared with those shown for AOD. Obviously, the R correlation coefficient presents very low values, which are below 0.5 (the poor correlation is observed in the scatter plots similar to those in Figure 6, not shown here). Excluding AE_t and AE_a values equal to 1.5 or 1.8 entails no substantial difference, only lower BIAS values. Overall, the results of the comparison showed the low quantitative skill of the AE_t and AE_a for this site. One factor contributing to this result is that the AE from the MODIS DB algorithm displays

great uncertainty for low-AOD conditions, since AE is obtained as a gradient between two small AOD numbers (Wagner and Silva, 2008).

3.4 Comparison of AOD between MODIS products and BAOD for the four Cuban actinometrical stations.

Two main facts limit the number of available BAOD values coincident in time with AOD_t and AOD_a: the hourly time step between manual DNI observations and the required condition of a clear line of sight between the pyrheliometer and a region of 5° around the Sun. Consequently, only one BAOD measurement could coincide each day with AOD_t, and another with AOD_a given the time coincidence criteria. Table 7 lists the number of coincident AOD_t, AOD_a, AOD_{ta} observations in space and time with BAOD both for the DB and DT algorithms for each of the actinometrical stations. Since the amount of coincident observations at each station is low, we decided to combine all the pairs of AOD_t, AOD_a and AOD_{ta} coincident with BAOD in the four sites together in order to conduct the comparison. In addition, we did not consider the very few cases with values of BAOD > 0.6, around 1 % of all cases, so as to avoid the possibility of inadvertent cloud contamination.

Table 8 contains almost the same statistics used in previous comparison satellite-sun photometer data (see Table 4 and 5), both for the DB and for DT algorithms for the four actinometrical stations together. The only statistic not included in Table 8 is f, the fraction of the MODIS/AERONET AOD retrievals in agreement within the expected uncertainty, because such uncertainty still has to be established for BAOD. We highlighted the best performing algorithm in bold for each of the statistics. The AOD_a derived with the DB algorithm performs better than the other three combinations of AOD_t, AOD_a, for DT and DB in accordance with all four statistics, except for BIAS, where the best performing is still the DB algorithm, but for AOD_t. However, in

general and taking into account the low number of data and the fact that we have single observations, the RMSE, MAE and BIAS for AOD_t, AOD_a, AOD_{ta} derived with both DB and DT algorithms remain in the same order of magnitude as earlier Tables 4 and 5, with the exception of the low values of the correlation coefficient R. The BIAS shows almost similar behavior except for its best performing value. This different behavior of algorithms and platforms with respect to the earlier results of Table 4-5 is clearly shown by Figure 6 where the scatter plots of the BAOD vs. AOD_t, AOD_a, and AOD_{ta} are depicted. What is clear is the poor correlation given by the very low values of the slope with respect to the value 1 and also the relatively high values of the intercept in relation to 0, and hence the resulting low values of the R coefficient. BAOD shows a high uncertainty for low values of AOD (below 2, see this range over the X axis in the plots) which are those prevalent in this area (l).

4. Conclusions

This study addresses the comparisons of different sources of AOD and AE from ground-based sun photometer (AERONET level 2.0 data), MODIS instruments (Terra, Aqua, and Terra + Aqua) and retrievals from direct normal solar irradiance observations in Cuba.

The comparison of spatial and temporal coincident single observations and collocated daily means of AOD_t, AOD_a, AOD_{ta} vs. AOD_{SP} shows, in general, a better performance for the Dark Target (DT) than for the Deep Blue (DB) algorithm for Camagüey. In particular we found: 1) small differences were found between AOD_t and AOD_a, thus justifying the combination of these observations in a single dataset for climatological studies; 2) Both DT and DB algorithms are better than expected (f around 80%) between November and January, but in other months f is on the order of one standard deviation (f = 68%) for DT and significantly lower for DB; 3) from linear

correlation analysis, MODIS slightly overestimates AOD compared to the sun photometers; 4) data from both MODIS instruments are well correlated with AERONET AOD with regression slopes close to 1, with the DT algorithm outperforming the DB algorithm; In addition, the comparison of multi-annual monthly means of AODta with AODsp indicate better agreement with results from the DT algorithm (compared to DB), consistent with the findings above.

The Ångström exponents AE_t, AE_a and AE_{ta} do not show good agreement with the spatial and temporal coincident AE_{SP} values when the default-1.5 and the constrained-1.8 values are or are not considered. Those results corroborate the limited skills of the MODIS derived AE, as indicated in previous studies.

In the comparison of BAOD vs. AOD_t, AOD_a, AOD_{ta}, where only individual observations can be compared, the statistics indicate larger uncertainties but of the same order of magnitude as the statistics of MODIS-photometer. Although correlations are very poor, these results support the potential of BAOD as a reliable source of aerosol information for climatological studies in areas that lack a sun photometer or any other surface aerosol measurement.

5. Acknowledgements:

This work has been supported by the Cuban National Program "Meteorology and sustainable development for Cuba" research grant P211LH007-20 and by the Joint Agreement between the University of Valladolid, Spain, and the Cuban Meteorological Institute for aerosol research. JCAM wishes to thank Dr. Loraine Remer and Dr. Andrew Sayer for their contributions to understanding MODIS algorithms. This research has received funding from the European Union's Horizon 2020 Research and Innovation Program under grant agreement No 654109

(ACTRIS-2). We acknowledge the funding provided by MINECO (CTM2015-66742-R) and by the Junta de Castilla y León (VA100U14).

6. References:

Antuña, J. C., Fonte, A., Estevan, R., Barja, B., Acea, R., Antuña Jr.: J.C., Solar radiation data rescue at Camagüey, Cuba, *Bull. Am. Meteorol. Soc*, **89**, 1507–1511. http://dx.doi.org/10.1175/2008BAMS2368.1, 2008.

Antuña J. C., Hernández, C., Estevan, R., Barja, B., Fonte, A., Hernández, T., Antuña Jr, J. C.: Camagüey's solar radiation rescued dataset: preliminary applications, *Óptica Pura y Aplicada*, **44** (1), 43-48, 2011.

Antuña, J. C., Estevan, R., Barja, B.: Demonstrating the Potential for First-Class Research in Underdeveloped Countries: Research on Stratospheric Aerosols and Cirrus Clouds Optical Properties, and Radiative Effects in Cuba (1988–2010), *Bull. Amer. Meteor. Soc.*, **93**, 1017–1027. http://dx.doi.org/10.1175/BAMS-D-11-00149.1, 2012.

Antuña-Marrero, J. C., De Frutos Baraja, A., Estevan Arredondo, R.: Joint aerosol research between Cuba and Spain proves fruitful, *EOS*, **97**, doi:10.1029/2016EO060125, 2016.

Barja, B., Rosas, J., Estevan, R.: Caracterización del contenido integral del vapor de agua atmosférico sobre Cuba obtenido mediante mediciones y modelación, Scientific Report, Grant 200.04070, 77 pp. (In Spanish, unpublished), 2015.

Bennouna, Y. S., Cachorro, V. E., B., Toledano, C., Berjon, Prats, N., D Fuertes, González, R.; Rodrigo, R., Torres, B., and De Frutos, A. M.: Comparison of atmospheric aerosol climatologies over southwestern Spain derived from AERONET and MODIS. Remote Sens. Environ. 115, 1272-1284, 2011, doi:10.1016/j.rse.2011.01.011.

Bennouna, Y. S., Cachorro, V. E., Torres, B., Toledano, C., Berjon, A., de Frutos, A. M. and Alonso Fernandez-Coppel, I.: Atmospheric turbidity determined by the annual cycle of the

aerosol optical depth over north-center Spain from ground (AERONET) and satellite (MODIS). Atmos. Environ. 67, 353-364, 2013. doi:10.016./j.atmosenv.2012.10.065.

Denjean, C., Formenti, P., Desboeufs, K., Chevaillier, S., Triquet, S., Maillé, M., Cazaunau, M., Laurent, B., Mayol-Bracero, O.L :, Vallejo, P., Quiñones, M., Gutierrez-Molina, I. E., Cassola, F., Prati, P., and Andrews, E., and Ogren, J. : Size distribution and optical properties of Africanm mineral dust after intercontinental transport, *J. Geophys.* Res., 121, 7117–7138, doi:10.1002/2016JD024783. 2016.

Eck, T., Holben, B., Reid, J. Dubovik, O.: Wavelength dependence of the optical depth of biomass burning, urban, and desert dust aerosols. *J. Geophys. Res.*, **104**, 31333_31349, 1999.

Estevan, R.: Certificación de depósito legal facultativo de obras protegidas; software: "Actino 2.0"; CENDA 218-2010. *(In Spanish)*, 2010.

Estevan R., Antuña, J.C., Barja, B., Hernández, C.E., Hernández, T., García, F., Rosas, J., Platero, I. Y.: Climatología de la Radiación solar en Camagüey 1981 – 2010, *Scientific Report*, Grant 01301216, 41 pp. (*In Spanish, unpublished*), 2016.

Fonte, A., Antuña, J.C.: Caracterización del espesor óptico de banda ancha de los aerosoles troposféricos en Camagüey, Cuba, *Revista Cubana de Meteorología*, **17**, No. 1, pp. 15-26, 2011.

García, F., Estevan, R., Antuña-Marrero, J. C., Rosas, J., Platero, I. Y., Antuña-Sánchez, J., C. Díaz, N.: Determinación de la Línea Base del Espesor Óptico de Aerosoles de Banda Ancha y comparación con datos de fotómetro solar. *Óptica Pura y Aplicada*, **48**(4), 249-258.doi: 10.7149/OPA.48.4.249, 2015.

GGO: Manual for the setup and operation of solar radiation instruments. Ed. Guidrometeoizdat, 124 pp. *(In Russian),* 1957.

Gkikas, A., Hatzianastassiou, N., Mihalopoulos, N., Katsoulis, V., Kazadzis, S., Pey, J., Querol, X., and Torres, O.: The regime of intense desert dust episodes in the Mediterranean based on contemporary satellite observations and ground measurements, *Atmos. Chem. Phys.*, *13*(23), 12135-12154, doi:10.5194/acp-13-12135-2013, 2013.

Gkikas, A., Basart, S., Hatzianastassiou, N., Marinou, E., Amiridis, V., Kazadzis, S., Pey, J., Querol, X., Jorba, O., Gassó, S., and Baldasano, J. M.: Mediterranean desert dust outbreaks and their vertical structure based on remote sensing data, *Atmos. Chem. Phys. Discuss.*, 15, 27675-27748, doi:10.5194/acpd-15-27675-2015, 2015.

GOAC: Manual de Observaciones Actinométricas, 37 pp. (*In Spanish, unpublished*), 2010.

Gueymard, C.A.: Turbidity determination from broadband irradiance observations: A detailed multicoefficient approach. *J. Appl. Meteorol*. **37**: 414-435, 1998.

Gueymard, C. A.: Aerosol turbidity derivation from broadband irradiance observations: Methodological advances and uncertainty analysis. *Solar 2013 Conf.*, Baltimore, MD, American Solar Energy Soc., 8 pp., 2013.

Holben, B. N., Tanré, D., Smirnov, A., Eck, T. F., Slutsker, I., Abuhassan, N., Newcomb, W. W., Schafer, J., Chatenet, B., Lavenue, F., Kaufman, Y. J., Castle, J. V., Setzer, A., Markham, B., Clark, D., Frouin, R., Halthore, R., Karnieli, A., O'Neill, N. T., Pietras, C., Pinker, R. T., Voss, K., Zibordi, G.: An emerging ground-based aerosol climatology: Aerosol optical depth from AERONET, *J. Geophys. Res.*, **106**, 12,067–12,097, 2001.

Hsu, N. C., Tsay, S. C., King, M. D., Herman, J. R.: Aerosol Properties Over Bright-Reflecting Source Regions, *IEEE T. Geosci. Remote*, **42**, 557–569, doi:10.1109/TGRS.2004.824067, 2004.

Hsu, N. C., Tsay, S. C., King, M. D., Herman, J. R.: Deep blue retrievals of Asian aerosol properties during ACE-Asia, *IEEE T. Geosci. Remote*, **44**, 3180–3195, doi:10.1109/TGRS.2006.879540, 2006.

675 Hsu, N. C., Jeong, M.-J., Bettenhausen, C., Sayer, A. M., Hansell, R., Seftor, C. S., Huang, J.,
676 Tsay, S.-C.: Enhanced Deep Blue aerosol retrieval algorithm: the second generation, *J.*
677 *Geophys. Res.*, **118**, 9296–9315, doi:10.1002/jgrd.50712, 2013.
678 IPCC: Climate Change 2013. The Physical Science Basis –Contribution of Working Group I to
679 the Fifth Assessment Report of the Intergovernmental Panel on Climate Change, Stocker
680 TF, Qin D, Plattner G-K, Tignor M, Allen SK, Boschung J, Nauels A, Xia Y, Bex V,
681 Midgley PM. (eds). Cambridge University Press: Cambridge, UK and New York, NY,
682 2013.
683 Kahn, R. A., M. J. Garay, D. L. Nelson, R. C. Levy, M. A. Bull, D. J. Diner, J. V. Martonchik, E.
684 G. Hansen, L. A. Remer, and D. Tanré, Response to "Toward unified satellite climatology
685 of aerosol properties: 3. MODIS versus MISR versus AERONET", *J. Quant. Spectrosc.*
686 *Radiat. Transfer,* **112**(5), 901–909, doi:10.1016/j.jqsrt.2010.11.001, 2011.
687 Kaufman, Y. J., Wald, A. E., Remer, L. A., Gao, B.-C., Li, R.-R. and Flynn, L.: The MODIS 2.1-
688 μm channel-correlation with visible reflectance for use in remote sensing of aerosol, *IEEE*
689 *T. Geosci. Remote*, **35**, 1286–1298, doi:10.1109/36.628795, 1997a.
690 Kaufman, Y. J., Tanré, D., Remer, L. A., Vermote, E. F., Chu, A., Holben, B. N.: Operational
691 remote sensing of tropospheric aerosol over land from EOS moderate resolution imaging
692 spectroradiometer, *J. Geophys. Res*., **102**, 17051–17068, doi:10.1029/96JD03988, 1997b.
693 Kaufman, Y. J., Koren, I., Remer, L., Tanré, D., Ginoux, P., and Fan, S.: Dust transport and
694 deposition observed from the Terra-Moderate Resolution Imaging Spectroradiometer
695 (MODIS) spacecraft over the Atlantic Ocean. *J. Geophys. Res. Atmos.*, 110, D10S12, 2005.

Kirilov, T. B., Vlasov, Yu. B., Flaum, M. Ya.: Manual para la operación e instalación de instrumentos de radiación solar, Ed.Guidrometeoizdat, Leningrad, 124 pp. (In Russsian), 1957.

Knippertz, P., Stuut, J.-B.W., 2014. Chapter 1 Introduction. In: Knippertz, P., Stuut, J.-B.W. (Eds.), Mineral Dust: A Key Player in the Earth System. Springer, New York, pp. 1–14, http://dx.doi.org/10.1007/978-94-017-8978-3, 2014.

Levy, R. C., Remer, L., Mattoo, S., Vermote, E., and Kaufman, Y.: Second-generation operational algorithm: Retrieval of aerosol properties over land from inversion of moderate resolution imaging spectroradiometer spectral reflectance. *J. Geophys. Res. Atmos.*, **112**, D13211, 2007.

Levy, R. C., Leptoukh, G., Kahn, R., Zubko, V., Gopalan, A., and Remer, L.: A critical look at deriving monthly aerosol optical depth from satellite data. *IEEE Transactions on Geoscience and Remote Sensing*, **47**(8), 2942−2956, 2009.

Levy, R. C., Remer, L. A., Kleidman, R. G., Mattoo, S., Ichoku, C., Kahn, R., Eck, T. F.: Global evaluation of the Collection 5 MODIS dark-target aerosol products over land, *Atmos. Chem. Phys.*, **10**, 10399-10420, doi:10.5194/acp-10-10399-2010, 2010.

Levy, R. C., Mattoo, S., Munchak, L. A., Remer, L. A., Sayer, A. M., Patadia, F., Hsu, N. C.: The Collection 6 MODIS aerosol products over land and ocean, *Atmos. Meas. Tech.*, **6**, 2989-3034, doi:10.5194/amt-6-2989-2013, 2013.

Levy, R. C., Munchak, L.A., Mattoo, S., Patadia, F., Remer, L.A., and Holz, R. E.: Towards a long-term global aerosol optical depth record: applying a consistent aerosol retrieval algorithm to MODIS and VIIRS-observed reflectance. *Atmos. Meas. Tech.*, **8**, 4083–4110, 2015. doi:10.5194/amt-8-4083-2015.

719 Long, C. N., Shi, Y.: The QCRad Value Added Product: Surface Radiation Measurement Quality
720 Control Testing, Including Climatology Configurable Limits, Office of Biological and
721 Environmental Research, U.S. Department of Energy, pp. 69, 2006.
722 Long, C. N., Shi, Y.: An Automated Quality Assessment and Control Algorithm for Surface
723 Radiation Observations. *The Open Atmospheric Science Journal*, **2**, 23-37, 2008.
724 Martínez, E., Campos, A., Borrajero, I., Vázquez, A.: Algunos índices de turbidez del aire en la
725 Ciudad de la Habana, *Revista Cubana de Meteorología*, **1** (1), pp. 57-60, 1988.
726 Mielonen, T., Levy, R. C., Aaltonen, V., Komppula, M., de Leeuw, G., Huttunen, J., Lihavainen,
727 H., Kolmonen, P., Lehtinen, K. E. J., Arola, A.: Evaluating the assumptions of surface
728 reflectance and aerosol type selection within the MODIS aerosol retrieval over land: the
729 problem of dust type selection, *Atmos. Meas. Tech.*, **4**, 201–214, doi:10.5194/amt-4-201-
730 2011, 2011.
731 Mishchenko M.I., Li Liu, Geogdzhayev, I. V., Travis, L. D., Cairns, B., Lacis, A. A.: Toward
732 unified satellite climatology of aerosol properties.: 3. MODIS versus MISR versus
733 AERONET, *J. Quant. Spectrosc. Radiat. Transfer*, 111, 540-552, 2010.
734 Ohmura, A., Dutton, E., Forgan, B., Froehlich, C., Gilgen, H., Hegner, H., Heimo, A., Koenig-
735 Langlo, G., McArthur, B., Mueller, G., Philipona, R., Pinker, R., Whitlock, C., Wild, M.:
736 Baseline Surface Radiation Network (BSRN/WCRP), a new precision radiometry for
737 climate research. *Bull. Am. Meteorol. Soc*., **79**, 2115-2136, 1998.
738 Papadimas, C.D., Hatzianastassiou, N., Mihalopoulos, N., Kanakidou, M., Katsoulis, B. D., and
739 Vardavas, I.: Assessment of the MODIS Collections C005 and C004 aerosol optical depth
740 products over the Mediterranean basin, Atmos. Chem. Phys., 9, 2987-2999;
741 doi.org/10.5194/acp-9-2987-2009, 2009.

742 Prospero, J. M., Lamb, P. J.: African droughts and dust transport to the Caribbean: Climate change
743 implications. *Science*, **302**, 1024–1027, 2003.
744 Prospero, J. M., Mayol-Bracero, O. L.: Understanding the transport and impact of African dust on
745 the Caribbean Basin, *Bull. Am. Meteorol. Soc.*, **94**(9), 1329–1335, 2013.
746 Prospero, J. M., Collard, F.-X., Molinié, J., Jeannot, A.: Characterizing the annual cycle of African
747 dust transport to the Caribbean Basin and South America and its impact on the environment
748 and air quality, *Global Biogeochem. Cycles*, **29**, 757–773, doi:10.1002/2013GB004802,
749 2014.
750 Remer, L. A., Tanré, D., Kaufman, Y. J., Ichoku, C., Mattoo, S., Levy, R., Chu, D. A., Holben, B.
751 N., Dubovik, O., Smirnov, A., Martins, J.V., Li, R. R., Ahmad, Z.: Validation of MODIS
752 aerosol retrieval over ocean. *Geophys. Res. Lett.*, 29(12), 1618, 2002.
753 Remer, L. A., Kaufman, Y. J, Tanre, D., Mattoo, S., Chu, D. A., Martins, J. V., Li, R. R., Ichoku,
754 C., Levy, R. C., Kleidman, R. G., Eck, T.F., Vermote, E., Holben, B. N.: The MODIS
755 aerosol algorithm, products, and validation". *J. Atmos. Sci.*, 62(4), 947-973, 2005.
756 Remer, L. A., Tanré, D., Kaufman, Y., Levy, R., and Mattoo, S.: Algorithm for remote sensing of
757 tropospheric aerosol from MODIS: Collection 005. https://modis-
758 images.gsfc.nasa.gov/_docs/MOD04:MYD04_ATBD_C005_rev1.pdf.
759 Sayer, A. M., Hsu, N. C., Bettenhausen, C., Jeong, M.-J.: Validation and uncertainty estimates for
760 MODIS Collection 6 “Deep Blue” aerosol data, *J. Geophys. Res. Atmos.*, **118**, 7864–7872,
761 doi:10.1002/jgrd.50600, 2013.
762 Sayer, A. M., Munchak, L. A., Hsu, N. C., Levy, R. C., Bettenhausen, C., Jeong, M.-J.: MODIS
763 Collection 6 aerosol products: Comparison between Aqua’s e-Deep Blue, Dark Target, and

764 "merged" data sets, and usage recommendations, *J. Geophys. Res. Atmos.*, **119**, 13,965–
765 13,989, doi:10.1002/2014JD022453, 2014.
766 Santese, M., De Tomasi, M. F. and, Perrone, M. R.: AERONET versus MODIS aerosol parameter
767 at different spatial resolutions over southeast Italy, J. Geophys. Res., 112, D10214,
768 doi:10.1029/2006JD007742, 2007.
769 Seinfeld, J. H. and S. N. Pandis.: Atmospheric chemistry and physics: from air pollution to climate
770 change. 3rd edition, John Wiley & Sons, Inc., ISBN: 9781118947401, 1120 pp., 2016.
771 Smirnov, A., Holben, B. N., Eck, T. F.. Dubovik, O., Slutsker, I.: Cloud-screening and quality
772 control algorithms for the AERONET database, *Remote Sens. Environ.*, **73**(3), 337–349,
773 2000.
774 Swap, R., Garstang, M., Greco, S., Talbot, R., Kallberg, P.: Saharan dust in the Amazon basin.
775 *Tellus*, **44B**, 133–149, 1992.
776 Tanré, D., Kaufman, Y. J., Herman, M., Mattoo, S.: Remote sensing of aerosol properties over
777 oceans using the MODIS/EOS spectral radiances, *J. Geophys. Res.*, **102**, 16971–16988,
778 1997.
779 Velasco-Merino, C., Mateos, D., Toledano, C.; Prospero, J. M., Molinie, J., Euphrasie-Clotilde,
780 L., González, R., Cachorro, V. e., Calle, A., and De Frutos, A. M.: Impact of long-range
781 transport over the Atlantic Ocean on Saharan dust optical and microphysical properties.
782 *Atmos. Chem. Phys. Disc.*, https://doi.org/10.5194/acp-2017-1089, 2017
783 Wagner, F., and Silva A. M.: Some considerations about Ångström exponent distributions. *Atmos.*
784 *Chem. Phys.*, **8**, 481–489, 2008.

Witte, J. C., A.R. Douglass, A. da Silva, O. Torres, R.C. Levy, and B.N. Duncan, (2011). NASA A-Train and Terra observations of the 2010 Russian wildfires, *Atmos. Chem. Phys.*, 11, 9287-9301, doi:10.5194/acp-11-9287-2011, 2011.

Yu, H. , M. Chin, T. Yuan, H. Bian, L. A. Remer, J. M. Prospero, A. Omar, D. Winker, Y. Yang, Y. Zhang, Z. Zhang and C. Zhao, The fertilizing role of African dust in the Amazon rainforest: A first multiyear assessment based on data from Cloud-Aerosol Lidar and Infrared Pathfinder Satellite Observations, *Geophys. Res. Lett.*, **42**, 1984–1991, doi:10.1002/2015GL063040, 2015.

Zhao, T. X.-P., Stowe, L. L., Smirnov, A., Crosby, D., Sapper, J., McClain, C. R.: Development of a global validation package for satellite oceanic aerosol optical thickness retrieval based on AERONET observations and its application to NOAA/NESDIS operational aerosol retrievals, *J. Atmos. Sci.*, **59**, 294– 312, 2002.

Tables:

Table 1: Aerosol products from the MODIS Collection 6 dataset used in the present study

Product	Description
Deep_Blue_Aerosol_Optical_Depth_550_Land_Best_Estimate	Deep Blue AOT at 0.55 micron for land with higher quality data (Quality flag=2,3)
Deep_Blue_Angstrom_Exponent_Land	Deep Blue Angstrom Exponent for land with all quality data (Quality flag=1,2,3)
Optical_Depth_Land_And_Ocean	AOT at 0.55 micron for both ocean (Average) (Quality flag=1,2,3) and land (corrected) (Quality flag=3)

Table 2: Information about Cuban actinometrical stations operating under the Solar Radiation Diagnostic Service (SRDS). Available number of BAOD observations included in column 6 and the period covered in the last column.

Code	Station Name	Latitude	Longitude	Height (m)	No. Obs.	Period
78355	Camagüey (CMW)	21.42	-77.85	122 m	2495	2001-2015
78330	Jovellanos (JVN)	22.80	-81.14	23 m	1182	2010-2015
78342	Topes de Collantes (TPC)	21.92	-80.02	766 m	1358	2011-2015
78321	Santa Fé (LFE)	21.73	-82.77	32 m	1756	2011-2015

Table 3: Number of available non-negative AOD_a, AOD_t, AE_a and AE_t data spatially coincident with the Camagüey sunphotometer in a radius of 25 km for each retrieval algorithm, DB and DT for the whole period 2001-2015, as well as the period 2008-2014, when sunphotometer data, AOD_{SP} and AE_{SP}, are available.

Period	**2001-2015**			**2008-2014**		
Algorithm	**DB**		**DT**	**DB**		**DT**
Parameter	**AOD**	**AE**	**AOD**	**AOD**	**AE**	**AOD**
Terra	6884	8111	6311	3418	4024	3166
Aqua	2445	3909	2869	1329	1534	2093

Table 4: Statistics of the comparison between collocated daily means of AOD_t and AOD_a with AOD_{SP} and the combined AOD_{ta} .

	AOD_{SP} vs. AOD_t		AOD_{SP} vs. AOD_a		AOD_{SP} vs. AOD_{ta}	
	DB	**DT**	**DB**	**DT**	**DB**	**DT**
RMSE	0.084	0.060	0.065	0.062	0.078	0.061
MAE	0.062	0.045	0.046	0.047	0.056	0.046
BIAS	-0.053	-0.001	-0.033	0.006	-0.046	0.002
R	0.730	0.729	0.785	0.779	0.741	0.753
f	0.656	0.803	0.763	0.795	0.694	0.800
Cases	311	335	169	254	480	589

Table 5: Statistics of the comparison between collocated single observation of AOD_t and AOD_a with AOD_{SP} and combined AOD_{ta} .

	AOD_{SP} vs. AOD_t		AOD_{SP} vs. AOD_a		AOD_{SP} vs. AOD_{ta}	
	DB	**DT**	**DB**	**DT**	**DB**	**DT**
RMSE	0.081	0.061	0.063	0.064	0.076	0.062
MAE	0.059	0.046	0.044	0.050	0.054	0.047
BIAS	-0.048	0.007	-0.027	0.017	-0.042	0.010
R	0.716	0.701	0.817	0.794	0.744	0.742
f	0.664	0.773	0.773	0.784	0.699	0.777
Cases	880	900	419	500	1299	1400

Table 6: Statistics of the comparison between AE_t, AE_a and AE_{ta} with AE_{SP} for single observations and daily mean values.

	Single observations			**Single observations (Except AE 1.5 & 1.8)**			**Collocated daily means**			**Collocated daily means (Except AE 1.5 & 1.8)**		
	AE_t	AE_a	AE_{ta}	AE_t	AE_a	AE_{ta}	AE_t	AE_a	AE_{ta}	AE_t	AE_a	AE_{ta}
RMSE	0.637	0.692	0.658	0.575	0.609	0.587	0.637	0.659	0.645	0.548	0.578	0.561
MAE	0.494	0.553	0.516	0.446	0.496	0.464	0.490	0.512	0.498	0.431	0.466	0.445
BIAS	-0.327	-0.337	-0.331	-0.129	-0.101	-0.119	-0.398	-0.384	-0.393	-0.189	-0.139	-0.167
R	-0.187	-0.426	-0.272	-0.191	-0.444	-0.269	-0.259	-0.414	-0.308	-0.124	-0.400	-0.236
Cases	615	374	989	353	189	542	311	169	480	172	120	292

Table 7: Number of coincident cases of AOD_t, AOD_a, AOD_{ta} with BAOD both for the DB and for DT algorithms.

Station:	BAOD vs. AOD_t		BAOD vs. AOD_a		BAOD vs. AOD_{ta}	
	DB	**DT**	**DB**	**DT**	**DB**	**DT**
Camagüey	166	171	66	79	232	250
Topes de Collantes	112	138	49	76	161	214
Jovellanos	65	65	35	34	100	99
La Fe	34	66	46	85	80	151
All combined	377	440	196	274	573	714

Table 8: Statistics of the comparison between the single observations of BAOD at the four actinometrical stations coincident in space and time with the single observation (L2) of AOD_t, AOD_a and AOD_{ta}. In bold, the values of best agreement.

	Camagüey, La Fe, Topes de Collantes & Jovellanos					
	BAOD vs. AOD_t		BAOD vs. AOD_a		BAOD vs. AOD_{ta}	
	DB	**DT**	**DB**	**DT**	**DB**	**DT**
RMSE	0.080	0.087	**0.073**	0.088	0.078	0.088
MAE	0.055	0.063	**0.048**	0.066	0.052	0.064
BIAS	**0.001**	0.027	0.014	0.049	0.005	0.035
R	0.455	0.325	**0.501**	0.417	0.468	0.355
Cases	373	436	191	268	564	704

Figure and Captions:

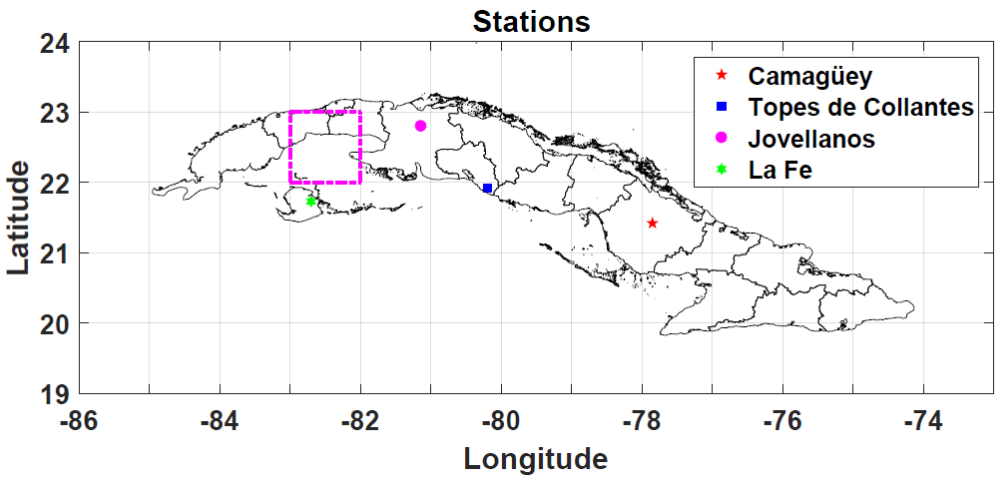

Figure 1: Map of Cuba locating the stations where the sun photometer and the four broadband pyrheliometer observations are conducted.

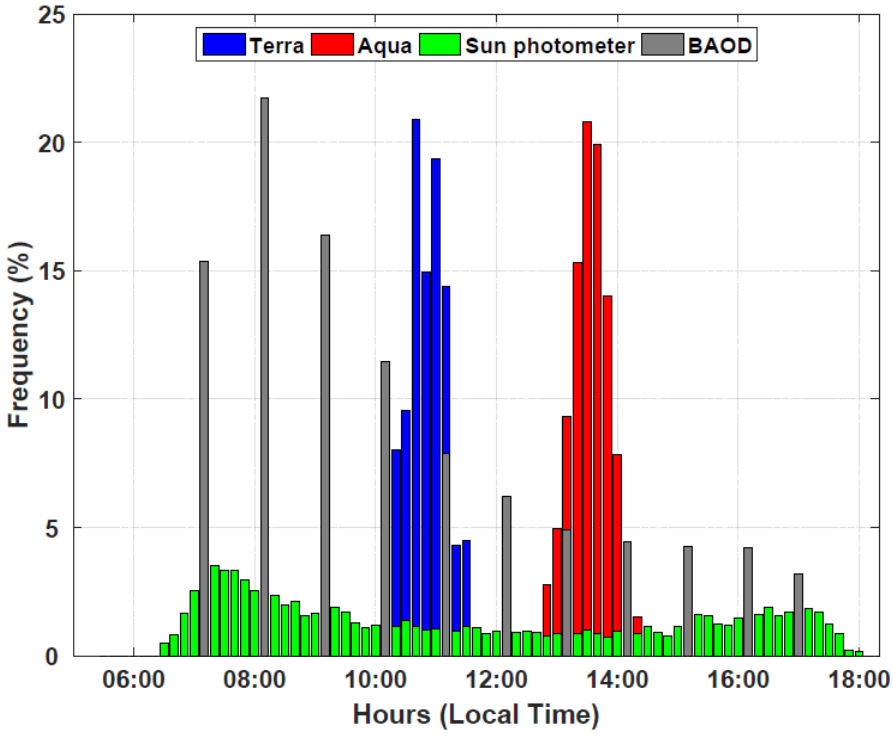

Figure 2: Frequencies of the time of the day (Local Time) overpass of Terra and Aqua (blue and red respectively) Camagüey's sun photometer site in a radius of 25 km for the period 2001 to 2015. In green the time frequencies for the Camagüey's sun photometer observations in the period 2008 to 2014. In addition, the time frequencies for the direct radiation observations used to calculate the BAOD. The bar width is 10 minutes for Terra, Aqua and the sun photometer and 1 hour for the BAOD.

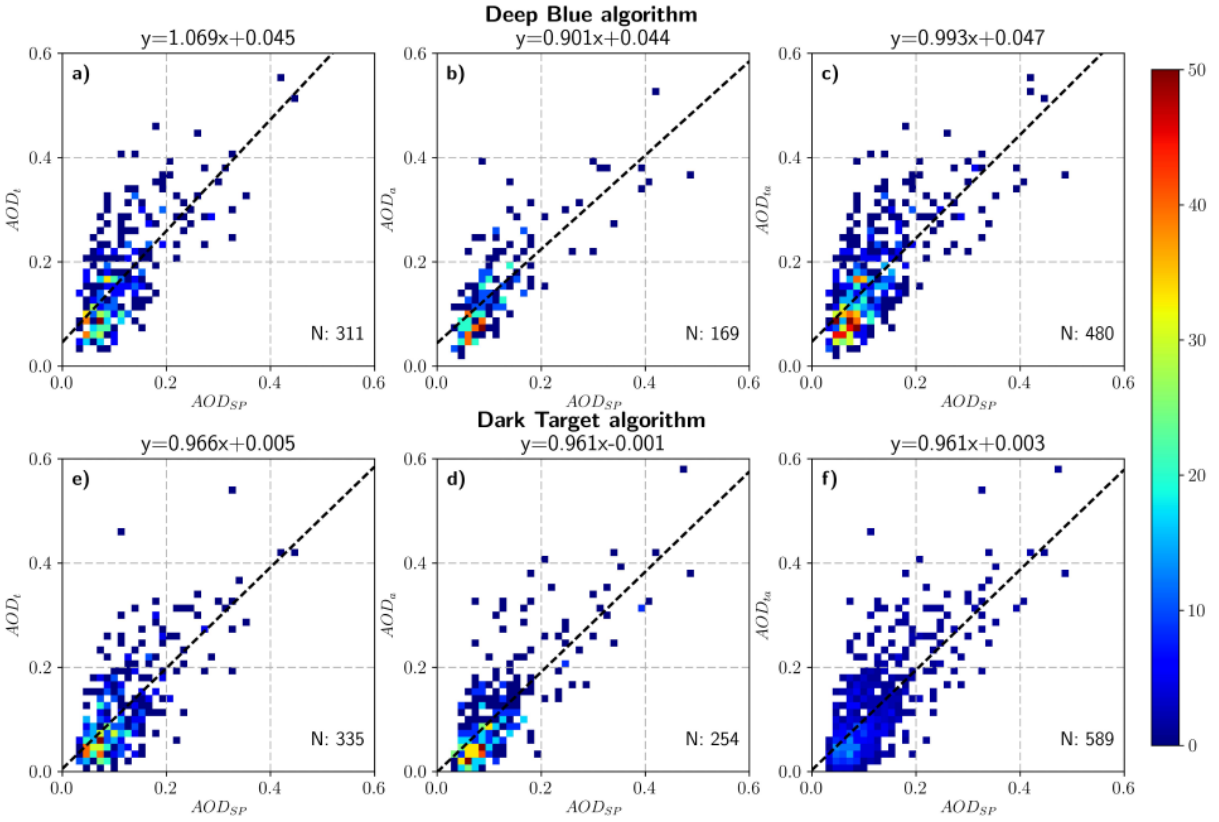

Figure 3: Collocated "daily mean" density scatter plots of the coincident AOD observations from the sun photometer and Terra and Aqua MODIS instruments for DB and DT algorithms.: a) to c) AOD_{SP} vs AOD_t , AOD_a and AOD_{ta} respectively for DB algorithm; d) to f) Idem for DT algorithm. The data density is represented by the color scale, showing the number of data points located in a particular area of the plot. Linear regression is given by the black discontinuous line and the corresponding equation. The number of data points appears in the right bottom.

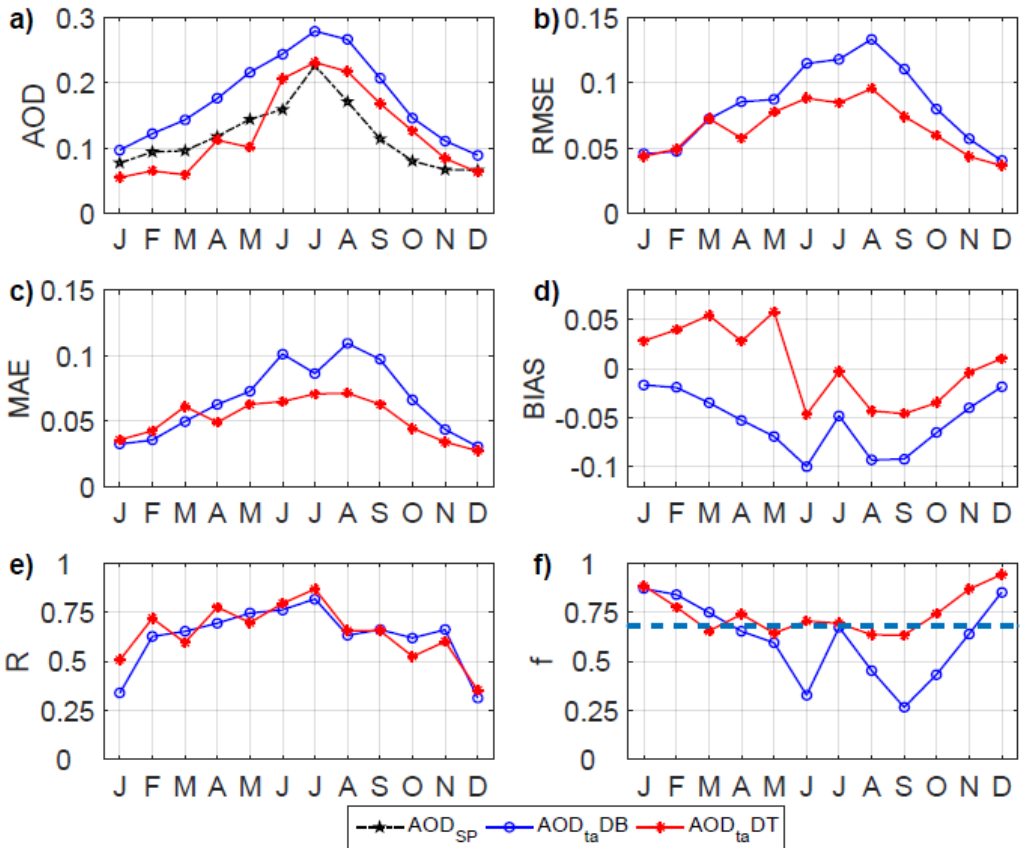

Figure 4: Monthly means and statistics (RMSE, MAE…….) resulting from the comparison between AOD_{SP} and AOD_{ta} for both DB and DT algorithms: a) Monthly means of the AOD_{SP} and AOD_{ta} for both DB and DT algorithms; b) RMSE for the comparison between AOD_{SP} and AOD_{ta} for both DB and DT algorithms; c) Idem for MAE, d) for BIAS, e) for R and f) for f. The blue discontinuous line at f= 68 % represent one standard deviation confidence interval for the EE indicator.

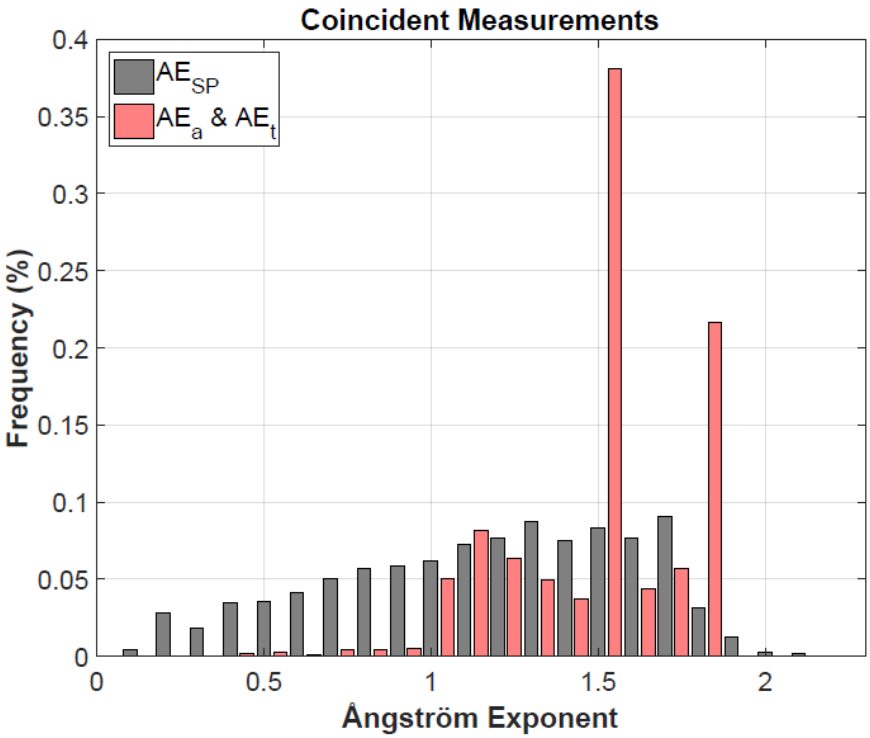

Figure 5: Frequency distribution of the Angstrom exponent (AE) values from both MODIS instruments Terra and Aqua and the sun photometer coincident in ± 30 minutes and 25 km radius around Camagüey.

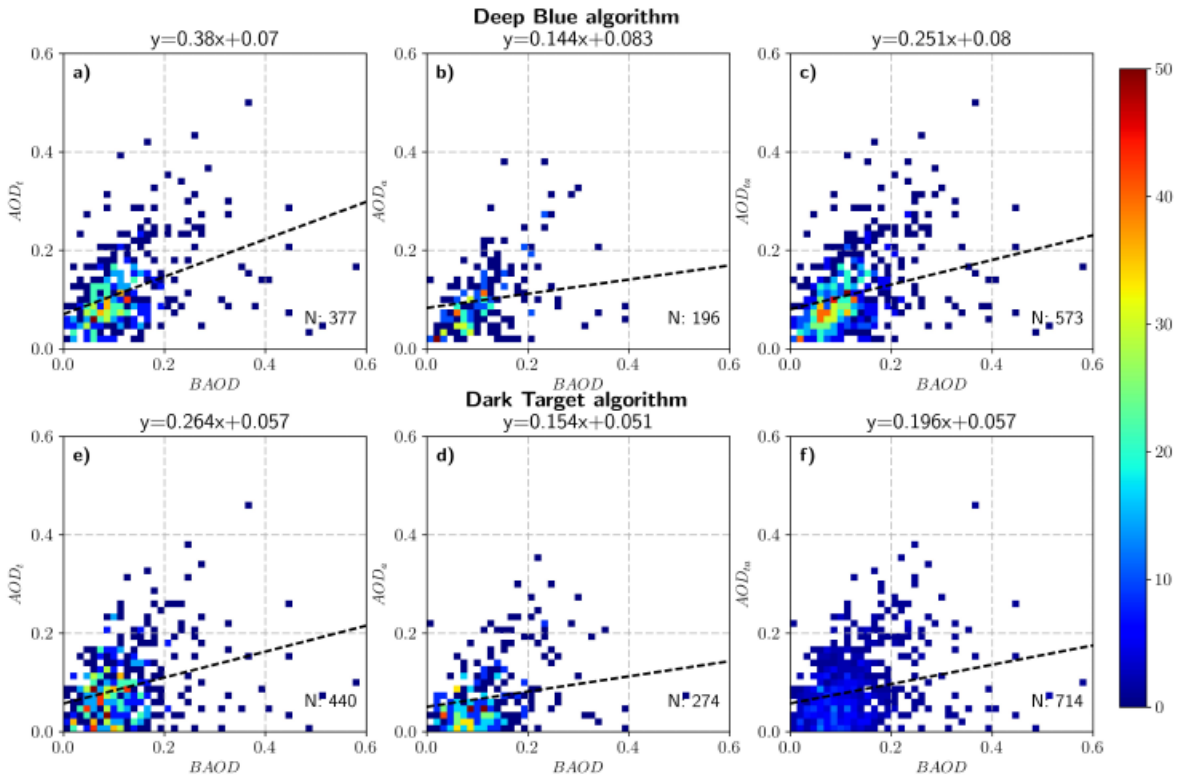

Figure 6: Single observations density scatter plots of the coincident BAOD observations from the broadband pyrheliometer and Terra and Aqua MODIS instruments for DB and DT algorithms.: a) to c) BAOD vs. AOD_t , AOD_a and AOD_{ta} respectively for DB algorithm; d) to f) Idem for DT algorithm. The data density is represented by the color scale, showing the number of data points located in a particular area of the plot. Linear regression line is shown by the black discontinuous line and the corresponding equation. The number of data points appears in the right bottom.